Efficient Generation of an Array of Single Silicon-Vacancy Defects in Silicon Carbide

Junfeng Wang,[1] Yu Zhou,[1] Xiaoming Zhang,[1] Fucai Liu,[2] Yan Li,[3] Ke Li,[1] Zheng Liu,[2] Guanzhong Wang,[4,*] and Weibo Gao[1,†]

[1]*Division of Physics and Applied Physics, School of Physical and Mathematical Sciences, Nanyang Technological University, Singapore 637371, Singapore*

[2]*Center for Programmable Materials, School of Materials Science & Engineering, Nanyang Technological University, 50 Nanyang Avenue, Singapore 639798, Singapore*

[3]*Key Lab of Quantum Information, CAS, University of Science and Technology of China, Hefei, Anhui, 230026, People's Republic of China*

[4]*Hefei National Laboratory for Physical Science at Microscale, and Department of Physics, University of Science and Technology of China, Hefei, Anhui, 230026, People's Republic of China*

(Received 21 December 2016; revised manuscript received 14 April 2017; published 16 June 2017)

Color centers in silicon carbide have increasingly attracted attention in recent years owing to their excellent properties such as single-photon emission, good photostability, and long spin-coherence time even at room temperature. As compared to diamond, which is widely used for hosting nitrogen-vacancy centers, silicon carbide has an advantage in terms of large-scale, high-quality, and low-cost growth, as well as an advanced fabrication technique in optoelectronics, leading to prospects for large-scale quantum engineering. In this paper, we report an experimental demonstration of the generation of a single-photon-emitter array through ion implantation. V_{Si} defects are generated in predetermined locations with high generation efficiency (approximately $19\% \pm 4\%$). The single emitter probability reaches approximately $34\% \pm 4\%$ when the ion-implantation dose is properly set. This method serves as a critical step in integrating single V_{Si} defect emitters with photonic structures, which, in turn, can improve the emission and collection efficiency of V_{Si} defects when they are used in a spin photonic quantum network. On the other hand, the defects are shallow, and they are generated about 40 nm below the surface which can serve as a critical resource in quantum-sensing applications.

DOI: 10.1103/PhysRevApplied.7.064021

I. INTRODUCTION

Silicon carbide (SiC) stands out for its application in quantum science in recent years due to its outstanding features. The main driving force behind exploring SiC comes from its advantage in chip integration over diamond, another material which is used widely to host a nitrogen-vacancy center. The same as diamond, SiC is a group-IV material, making it a nuclear-spinless environment to protect the coherence of color-center electron spins. Compared to diamond, the unique property of SiC includes high-quality, large wafer-scale growth, and mature nanofabrication and doping techniques [1–17]. SiC has been explored to generate single-photon emission in the visible [7,8] as well as near-infrared range [4,6]. Thanks to the possibility of SiC-doping control, an electrically driven SiC single-photon emitter has been created with the fabrication of emitting diodes [12]. In addition to its photonic properties similar to the nitrogen-vacancy centers in diamond [18], silicon-vacancy (V_{Si}) and -divacancy defects can be used as spin-qubit carriers and can be optically polarized and controlled by microwaves [1–3,5,6,9,10,13]. For V_{Si} defects, the coherent control of a single spin has been achieved at room temperature, and the coherence time reaches about 160 μs [3]. Moreover, the coherence time of the V_{Si} defect ensemble has been improved to abou`t 20 ms using dynamical decoupling at cryogenic temperature [15]. In particular, the V_{Si} defect has also been shown to be promising for the quantum sensing of magnetic field [9,11] and temperature [9].

For its application in quantum-information science, efficient generation of a single defect and single-photon source in SiC are required. Recently, two methods have been developed to generate single V_{Si} defects: high-energy electron irradiation [3] and neutron irradiation [4]. However, in both methods, the generation efficiency of the single V_{Si} defects is low, and the positions of the single V_{Si} defects are randomly distributed. For application in a spin photonics network [19], the creation of defects in well-defined locations is essential in order to enhance their emission efficiency by integrating them into photonic structures.

In this work, we experimentally realize the efficient generation of a nanoscale single V_{Si}-defect array in SiC. The V_{Si}-defect array is created by using 30-keV carbon ion implantation through an array of (65 ± 10)-nm-diameter

*Corresponding author.
gzwang@ustc.edu.cn
†wbgao@ntu.edu.sg

apertures patterned on a PMMA layer using electron-beam lithography (EBL) deposited on top of the SiC surface [20]. We first measure the photoluminescence (PL) spectrum and second-order autocorrelation function $g^2(t)$ of the defect emission at room temperature and confirm that they are single defects. We then study their saturation behavior and photostability, showing that the fluorescence emission is very stable without any indication of photoblinking. By sampling the V_{Si} defects on 100 implanted sites, we estimate that the efficiency of single silicon-vacancy defect generation is about $34\% \pm 4\%$, and the conversion yield of the implanted carbon ions into the V_{Si} defects is about $19\% \pm 4\%$. Finally, to confirm their origin further, we measure the PL spectrum and the optically detected magnetic resonance (ODMR) signal of the V_{Si} defects at both room temperature and low temperature (5 K).

II. EXPERIMENT

We first introduce the production steps for the defect centers. We start with a commercially available high-purity 4*H*-SiC epitaxy layer (its thickness is about 7 μm) sample. This ensures a low background suitable for single defect generation [3,4]. As shown in Fig. 1(a), after cleaning with acetone and isopropanol (IPA) in an ultrasonic bath, a 300-nm-thick PMMA layer ($A7:A4 = 5:3$) is deposited on the SiC surface by spin coating [20–22]. In the second step, an array of apertures with a 2-μm cell separation and some long 10-μm-wide strips used as position marks are generated using EBL [20]. After the development step, a series of holes are generated on the PMMA layer. With a scanning electron microscope (SEM), we can clearly see a hole about 65 ± 10 nm in diameter [Figs. 1(a) and 1(b)]. Afterwards, 30-keV C^+ ions are implanted with a fluence equal to 2.6×10^{11} C^+/cm^2 to generate the V_{Si}-defect array. The fluence corresponds to an average of around 8.6 carbons per aperture. Using SRIM (stopping and range of ions in matter) software simulation, we find that more than 99% of the 30-keV carbon atoms can be blocked by the PMMA layer, such that the defect can be implanted only through the apertures. After the implantation, the PMMA layer on the sample is removed by ultrasonication in acetone. Finally, the sample is cleaned by ultrasonication in IPA. In order to avoid the generation of other types of PL defects, the sample is not annealed [3]. Different from the generation of N-*V* center in diamond, the absence of annealing steps largely simplifies the production procedure. In order to estimate the accuracy of the V_{Si}-defect position, we consider the ion-straggling effect, simulated by SRIM software simulation. The average depth of the V_{Si} defects is about 42 nm, and the longitudinal straggling is about 35 nm.

III. RESULTS AND DISCUSSION

After the production process, we characterize the emission properties of the defects. First, we study the PL property of the emitters in a homemade confocal microscopy system [4]. A 690-nm continuous-wave laser is used to excite the V_{Si} defects through a high-N.A. (1.3) oil objective lens (Nikon). The fluorescent photons from the V_{Si} defects are collected by the same objective lens and transmitted through a dichroic mirror (801 nm). In order to suppress the background, the fluorescent photons are passed through a 75-μm-diameter pinhole between two lenses followed by a 900-nm long-pass filter. The photons are then directly detected by two avalanche photodiodes after a beam splitter in a Hanbury Brown and Twiss (HBT)

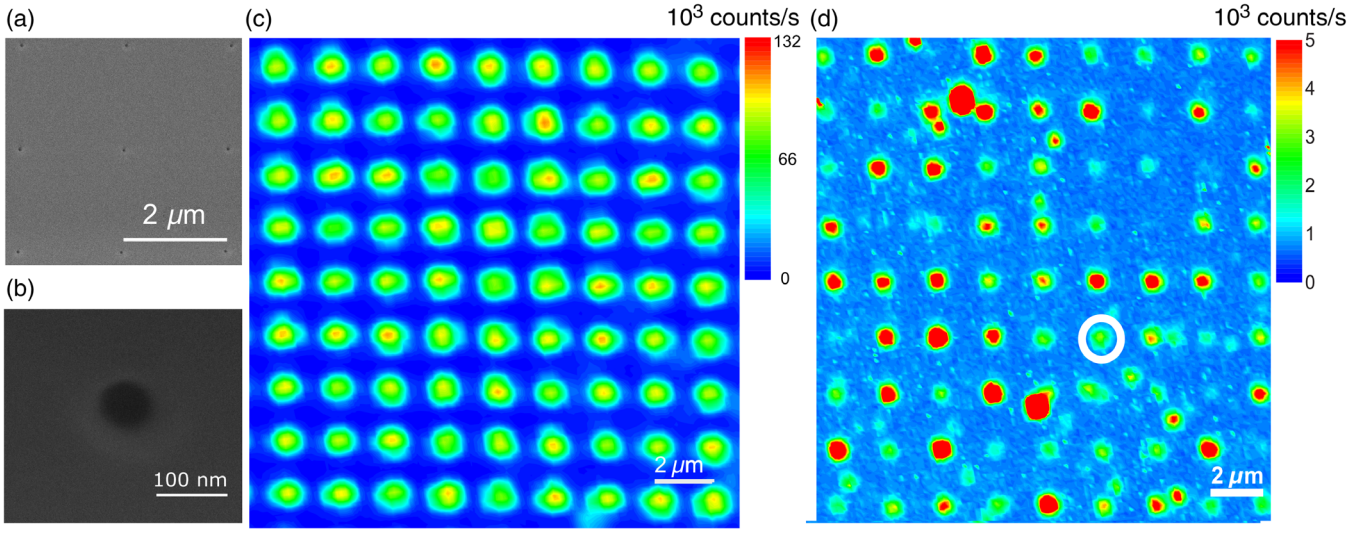

FIG. 1. (a) SEM image of aperture arrays with 2-μm cell separation patterned on the surface of the PMMA. (b) SEM image of an approximately 65-nm-diameter aperture patterned on the surface of the PMMA. (c) Confocal image of the sample area with large ion-implantation dose (3000 ions/aperture). (d) Confocal fluorescence image of the sample area with lower ion-implantation dose on the SiC surface. The circled one is the single V_{Si} defect that we study in this paper. The scale bar is 2 μm.

setup. PL count maps from two samples with different ion-implantation doses are shown in Figs. 1(c) and 1(d). As shown in this figure, the defect arrays can be seen clearly using the PL count map. The nearest two spots have a cell separation distance of 2 μm, which is consistent with the patterned PMMA apertures. The nonpatterned bright spots in Fig. 1(d) are V_{Si}-defect clusters formed during the implantation due to imperfect PMMA layers deposited on the SiC chip [20].

In order to infer the number of V_{Si} defects associated with the luminescent spots, we measure the second-order correlation function using the HBT setup. Since the saturation count for the single V_{Si} defect is about 7×10^3 counts/s, the signal-to-noise ratio is low (about 4 : 1), which will result in the correlation function being affected by the background noise. Here, the raw data $g^2(t)$ of the correlation function is corrected using the function $g^2{}_{corr}(t) = [g^2(t) - (1-\rho^2)]/\rho^2$, where $\rho = s/(s+b)$. Here, s and b are the signal and background count, respectively [4,6]. For the circled V_{Si} defect in Fig. 1(d), the value of ρ is about 0.8. Figure 2(a) shows the corrected correlation functions $g^2{}_{corr}(t)$ of the circled V_{Si} defect with 0.5-mW (black line) and 2-mW (red line) excitation power, respectively. The blue lines are the fit with the function $g^2{}_{corr}(t) = 1 - (1+a)\times \exp(-|\tau|/\tau_1) + a\exp(-|\tau|/\tau_2)$, where a, τ_1, and τ_2 are three fitting parameters. For the fitting function, we consider a three-level system with τ_1 and τ_2 related to the emission and shelving-state lifetimes [23,24]. Fitting curves are shown in Fig. 2(a), which agree with the single-emitter model for both excitation powers. For the 0.5-mW excitation, we have $a = 0.69 \pm 0.05$, $\tau_1 = 5.2 \pm 0.5$ ns, and $\tau_2 = 89.1 \pm 8.5$ ns; for 2-mW excitation, we have $a = 2.8 \pm 0.12$, $\tau_1 = 5.3 \pm 0.3$ ns, and $\tau_2 = 36.2 \pm 1.4$ ns.

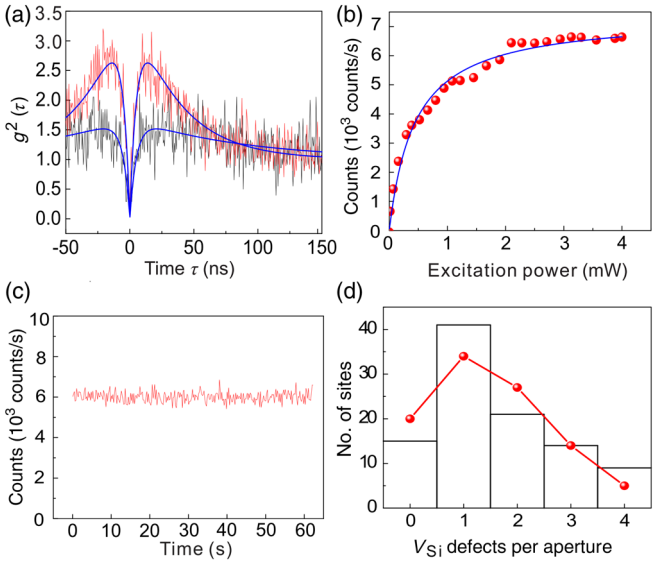

FIG. 2. (a) Second-order correlation function measurement with excitation power of 0.5 and 2 mW, respectively. The blue lines show the fitting of the data with the function introduced in the main text. (b) The PL count curve of the single V_{Si} defect as a function of the excitation power. (c) The PL count of the single V_{Si} defect as a function of time showing the photostability. The time bin is 100 ms and the excitation power is 2 mW here. (d) The histogram of the number of V_{Si} defects per aperture. The red line is the fit of the data by a Poisson distribution function.

We continue to show the saturation behavior of the single emitter. The PL saturation curve of the single V_{Si} defect as a function of excitation power P is presented in Fig. 2(b). The blue line is the theoretical fitting function $I(P) = I_s/(1 + P_0/P)$, where I_s is the maximum count, and P_0 is the saturation power. The maximum count I_s and the saturation power P_0 obtained from the fitting are 7.4×10^3 counts/s and 0.43 mW, respectively. Both values are of the same order as the previously published results [3,4]. Under a similar setup, the PL saturation count for single–N-V center in diamond can reach about 220×10^3 counts/s. Given their similar lifetimes, it remains an open question whether the reduced count rate comes from the trapping in other dark states. Since it is not uncommon for a solid-state emitter to have blinking behavior, we next study its photostability, which is much sought after in various quantum-information applications. Figure 2(c) shows the PL count time trace with 100-ms time bins under 2-mW excitation power. This figure indicates that there is no photoblinking for 60 s.

Since the saturation count of the single V_{Si} defect is only about 10×10^3 counts/s, the high-efficiency generation of the single V_{Si} defect in a predefined position is critical for its integration with photonic cavity waveguides to improve the emission and collection efficiency. In view of this problem, we give the statistics of the number of V_{Si} defects per implanted aperture, which is obtained by comparing the measured $g^2(0)$ values and PL intensity and the mean counts of a single V_{Si} defect. Figure 2(d) shows the histogram of 100 apertures. The red line is the Poissonian distribution-function fit of the data. The number of V_{Si} defects formed per aperture is 1.61 ± 0.32. Inferred from the fit, the single V_{Si}-defect generation ratio is $34\% \pm 4\%$. Since the implanted influence corresponds to about 8.6 carbon atoms per aperture, the conversion yield of the implanted carbon ions into the V_{Si} defects is about $19\% \pm 4\%$. The high conversion yield is comparable to the nitrogen implantation of the same energy used to generate the N-V center in diamond [20,25].

After the generation of the defect, we focus on characterizing the origin of the implanted defect. The first experiment is to measure the V_{Si}-defect ensemble of the 10-μm strip [20] PL spectrum at room temperature [Fig. 3(a)]. Here, the spectrum is cut by the 900-nm long-pass filter, which is used to block the laser and oil fluorescence background. At room temperature, the PL spectrum wavelengths range from 800 to 1100 nm, which is in the near-infrared range, which agrees with the room-temperature PL spectrum of the V_{Si} defect as measured in previous works [3,4,26]. We then measure the low-temperature (5-K) PL

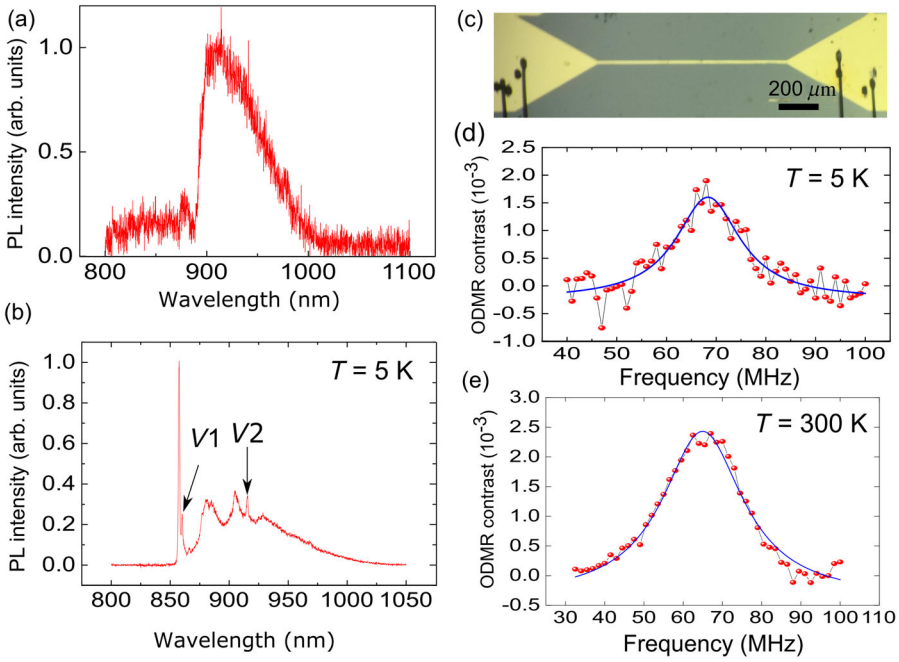

FIG. 3. (a) The PL spectrum of the V_{Si}-defect ensemble of the strip at room temperature. (b) Low-temperature (5-K) PL spectrum of the V_{Si}-defect ensemble of the strip. The $V1$ and $V2$ ZPLs of the V_{Si} defects are observed at 860.1 and 915.3 nm, respectively. (c) Fabricated microwave stripline on sample surface. (d) Cryogenic temperature ODMR measurement of the V_{Si}-defect ensemble on the strip at zero magnetic field. (e) Room-temperature ODMR measurement. The solid curve is the Lorentzian fitting to the spectrum.

spectrum. The V_{Si} defect is a point defect consisting of a silicon vacancy associated with four adjacent carbons in 4H-SiC. There are two types of V_{Si} defects in 4H-SiC: $V1$ and $V2$ centers. At cryogenic temperature, there are two zero-phonon lines (ZPLs), 861.4 and 916.3 nm, corresponding to the $V1$ and $V2$ centers, respectively [4,16]. A spectrum of a defect ensemble is shown in Fig. 3(b), from which we can see clearly the $V1$ and $V2$ peaks.

Last, we measure the continuous-wave ODMR for the implanted V_{Si} defects. Figure 3(c) shows a 20-μm-wide microwave stripline fabricated by standard EBL technology. Only the ODMR of the $V2$ center is studied in this work. Its negatively charged ground state is a spin quartet state with $S = 3/2$ exhibiting a zero-field splitting, and $D = 35$ MHz, which can be polarized by a laser and controlled by microwave [3,4,16]. Figures 3(d) and 3(e) show the ODMR measurement of the ensemble V_{Si} defects at cryogenic temperature and room temperature, respectively. According to the Lorentz fit of the data, we obtain the resonant frequency as 68.4 MHz with its linewidth (FWHM) 15.7 $\pm$ 1.8 MHz for low cryogenic temperature. For room temperature, the resonant frequency is at 65.1 MHz, and its linewidth (FWHM) is 25.0 $\pm$ 1.4 MHz, which is consistent with previous results [4,11]. The slight difference might come from residual strains in different samples, and the linewidth broadening can be affected by the decoherence of the spin qubits in the nonannealed implantation sample.

IV. SUMMARY

In summary, we experimentally demonstrate the generation of a single silicon-vacancy defect array in silicon carbide with high efficiency. The successful generation of a single silicon-vacancy defect in a well-defined position around tens of nanometers may open up several immediate research possibilities. First, a critical factor in quantum magnetometry with a color center is the closeness of the sensing defect to the surface [27]. This is because the dipolar magnetic fields decay as the third inverse power of the distance between the sensing spin and magnetic field target. We, therefore, need to have the defect centers close enough to the sample surface. The created shallow defects may find their application in nanoscale magnetometry, especially if it is combined with chemical etching [28–30]. Second, it might serve as an efficient way to engineer spin-spin entanglement through dipole-dipole coupling [31–33]. Again, because of the coupling decays as the distance between the two defect spins with d^{-3}, it is much more favorable to generate two defects close to each other in the production procedure. The possibility to generate a few defects in the tens of nanometers scale, as we demonstrate here, can be used towards this direction. Third, to precisely couple the single emitter to a photonic crystal cavity [12,34–36], solid immersion lenses [37], or nanopillar structures [38,39], one needs a precise location with accuracy in the order of tens of nanometers. The method we demonstrate here may ease the coupling of the emitter to the fabricated cavity or waveguide [34–36]. Finally, with modified parameters and possibly additional, annealing steps, similar production of other types of single defects, such as divacancies [1,2,6] and carbon antisite-vacancy pair defects [8] may become possible in future.

ACKNOWLEDGMENTS

We thank Phani Kumar and Abdullah Rasmita for discussions. We acknowledge the support from the Singapore National Research Foundation through a

Singapore 2015 NRF Fellowship Grant No. NRF-NRFF2015-03 and its Competitive Research Program (CRP Grant No. NRF-CRP14-2014-02), MOE tier 1 (Grant No. RG 176/15), NTU start-up Grant (M4081441) and the Astar QTE Project.

APPENDIX: ODMR MEASUREMENT

For the ODMR measurement, a 4-mW 690-nm laser above the objective is used to excite the defects. The microwave signal is generated by signal generator and then gated by a switch. After it is amplified by the amplifier, it is sent into a Montana cryostation and then fed to a microwave stripline. As shown in Fig. 3(b), the 20-μm-wide stripline is fabricated on the sample surface by the standard lithography method. The whole experiment is synchronized by pulse blaster. To decrease the fluctuation noise, ODMR scans from 40 to 100 MHz are conducted six times, and then the scan results are averaged. For one point in each scan, the microwave signal is gated on and off with 2.8-ms duration and repeated 20 000 times [16]. The photon counts in each on and off microwave period are recorded by a data acquisition card triggered by a pulse blaster. The final ODMR contrast is calculated by $\Delta\mathrm{PL} = [\Sigma N(\mathrm{on}) - \Sigma N(\mathrm{off})]/\Sigma N(\mathrm{off})$.

[1] W. F. Koehl, B. B. Buckley, F. J. Heremans, G. Calusine, and D. D. Awschalom, Room temperature coherent control of defect spin qubits in silicon carbide, Nature (London) **479**, 84 (2011).

[2] A. L. Falk, B. B. Buckley, G. Calusine, W. F. Koehl, V. V. Dobrovitski, A. Politi, C. A. Zorman, P. X.-L. Feng, and D. D. Awschalom, Polytype control of spin qubits in silicon carbide, Nat. Commun. **4**, 1819 (2013).

[3] M. Widmann, S.-Y. Lee, T. Rendler, N. T. Son, H. Fedder, S. Paik, L.-P. Yang, N. Zhao, S. Yang, I. Booker, A. Denisenko, M. Jamali, S. A. Momenzadeh, I. Gerhardt, T. Ohshima, A. Gali, E. Janzén, and J. Wrachtrup, Coherent control of single spins in silicon carbide at room temperature, Nat. Mater. **14**, 164 (2015).

[4] F. Fuchs, B. Stender, M. Trupke, D. Simin, J. Pflaum, V. Dyakonov, and G. V. Astakhov, Engineering near-infrared single-photon emitters with optically active spins in ultrapure silicon carbide, Nat. Commun. **6**, 7578 (2015).

[5] L.-P. Yang, C. Burk, M. Widmann, S.-Y. Lee, J. Wrachtrup, and N. Zhao, Electron spin decoherence in silicon carbide nuclear spin bath, Phys. Rev. B **90**, 241203(R) (2014).

[6] D. J. Christle, A. L. Falk, P. Andrich, P. V. Klimov, J. Ul Hassan, N. T. Son, E. Janzén, T. Ohshima, and D. D. Awschalom, Isolated electron spins in silicon carbide with millisecond coherence times, Nat. Mater. **14**, 160 (2015).

[7] B. Lienhard, T. Schröder, S. Mouradian, F. Dolde, T. T. Tran, I. Aharonovich, and D. Englund, Bright and photostable single-photon emitter in silicon carbide, Optica **3**, 768 (2016).

[8] S. Castelletto, B. C. Johnson, V. Ivády, N. Stavrias, T. Umeda, A. Gali, and T. Ohshima, A silicon carbide room-temperature single-photon source, Nat. Mater. **13**, 151 (2014).

[9] H. Kraus, V. A. Soltamov, F. Fuchs, D. Simin, A. Sperlich, P. G. Baranov, G. V. Astakhov, and V. Dyakonov, A magnetic field and temperature sensing with atomic-scale spin defects in silicon carbide, Sci. Rep. **4**, 5303 (2014).

[10] P. V. Klimov, A. L. Falk, B. B. Buckley, and D. D. Awschalom, Electrically Driven Spin Resonance in Silicon Carbide Color Centers, Phys. Rev. Lett. **112**, 087601 (2014).

[11] D. Simin, F. Fuchs, H. Kraus, A. Sperlich, P. G. Baranov, G. V. Astakhov, and V. Dyakonov, High-Precision Angle-Resolved Magnetometry with Uniaxial Quantum Centers in Silicon Carbide, Phys. Rev. Applied **4**, 014009 (2015).

[12] A. Lohrmann, N. Iwamoto, Z. Bodrog, S. Castelletto, T. Ohshima, T. J. Karle, A. Gali, S. Prawer, J. C. McCallum, and B. C. Johnson, Single-photon emitting diode in silicon carbide, Nat. Commun. **6**, 7783 (2015).

[13] P. V. Klimov, A. L. Falk, D. J. Christle, V. V. Dobrovitski, and D. D. Awschalom, Quantum entanglement at ambient conditions in a macroscopic solid-state spin ensemble, Sci. Adv. **1**, e1501015 (2015).

[14] H. Kraus, V. A. Soltamov, D. Riedel, S. Vath, F. Fuchs, A. Sperlich, P. G. Baranov, V. Dyakonov, and G. V. Astakhov, Room-temperature quantum microwave emitters based on spin defects in silicon carbide, Nat. Phys. **10**, 157 (2014).

[15] D. Simin, H. Kraus, A. Sperlich, T. Ohshima, G. V. Astakhov, and V. Dyakonov, Locking of electron spin coherence above 20 ms in natural silicon carbide, Phys. Rev. B **95**, 161201 (2017).

[16] S. G. Carter, O. O. Soykal, P. Dev, S. E. Economou, and E. R. Glaser, Spin coherence and echo modulation of the silicon vacancy in 4H-SiC at room temperature, Phys. Rev. B **92**, 161202(R) (2015).

[17] H. J. V. Bardeleben, J. L. Cantin, E. Rauls, and U. Gerstmann, Identification and magneto-optical properties of the NV center in 4H-SiC, Phys. Rev. B **92**, 064104 (2015).

[18] L. Childress, M. V. Gurudev Dutt, J. M. Taylor, A. S. Zibrov, F. Jelezko, J. Wrachtrup, P. R. Hemmer, and M. D. Lukin, Coherent dynamics of coupled electron and nuclear spin qubits in diamond, Science **314**, 281 (2006).

[19] W. B. Gao, A. Imamoglu, H. Bernien, and R. Hanson, Coherent manipulation, measurement and entanglement of individual solid-state spins using optical fields, Nat. Photonics **9**, 363 (2015).

[20] J. F. Wang, F. P. Feng, J. Zhang, J. H. Chen, Z. C. Zheng, L. P. Guo, W. L. Zhang, X. R. Song, G. P. Guo, L. L. Fan, C. W. Zou, L. R. Lou, W. Zhu, and G. Z. Wang, High-sensitivity temperature sensing using an implanted single nitrogen-vacancy center array in diamond, Phys. Rev. B **91**, 155404 (2015).

[21] D. M. Toyli, C. D. Weis, G. D. Fuchs, T. Schenkel, and D. D. Awschalom, Chip-scale nanofabrication of single spins and spin arrays in diamond, Nano Lett. **10**, 3168 (2010).

[22] P. Spinicelli, A. Dréau, L. Rondin, F. Silva, J. Achard, S. Xavier, S. Bansropun, T. Debuisschert, S. Pezzagna, J. Meijer, V. Jacques, and J.-F. Roch, Engineered arrays of nitrogen-vacancy color centers in diamond based on implantation of CN^- molecules through nanoapertures, New J. Phys. **13**, 025014 (2011).

[23] C. Kurtsiefer, S. Mayer, P. Zarda, and H. Weinfurter, Stable Solid-State Source of Single Photons, Phys. Rev. Lett. **85**, 290 (2000).

[24] E. Neu, D. Steinmetz, J. Riedrich-Möller, S. Gsell, M. Fischer, M. Schreck, and C. Becher, Single photon emission from silicon-vacancy colour centres in chemical vapour deposition nano-diamonds on iridium, New J. Phys. **13**, 025012 (2011).

[25] B. Naydenov, F. Reinhard, A. Lämmle, V. Richter, R. Kalish, U. F. S. D'Haenens-Johansson, M. Newton, F. Jelezko, and J. Wrachtrup, Increasing the coherence time of single electron spins in diamond by high temperature annealing, Appl. Phys. Lett. **97**, 242511 (2010).

[26] P. G. Baranov, A. P. Bundakova, A. A. Soltamova, S. B. Orlinskii, I. V. Borovykh, R. Zondervan, R. Verberk, and J. Schmidt, Silicon vacancy in SiC as a promising quantum system for single-defect and single-photon spectroscopy, Phys. Rev. B **83**, 125203 (2011).

[27] L. Rondin, J.-P. Tetienne, T. Hingant, J.-F. Roch, P. Maletinsky, and V. Jacques, Magnetometry with nitrogen-vacancy defects in diamond, Rep. Prog. Phys. **77**, 056503 (2014).

[28] S. Cui, A. S. Greenspon, K. Ohno, B. A. Myers, A. C. B. Jayich, D. D. Awschalom, and E. L. Hu, Reduced plasma-induced damage to near-surface nitrogen-vacancy centers in diamond, Nano Lett. **15**, 2887 (2015).

[29] J. F. Wang, W. L. Zhang, J. Zhang, J. You, Y. Li, G. P. Guo, F. P. Feng, X. R. Song, L. R. Lou, W. Zhu, and G. Z. Wang, Coherence times of precise depth controlled NV centers in diamond, Nanoscale **8**, 5780 (2016).

[30] F. Z. Shi, Q. Zhang, P. F. Wang, H. B. Sun, J. R. Wang, X. Rong, M. Chen, C. Y. Ju, F. Reinhard, H. W. Chen, J. Wrachtrup, J. F. Wang, and J. F. Du, Single-protein spin resonance spectroscopy under ambient conditions, Science **347**, 1135 (2015).

[31] P. Neumann, R. Kolesov, B. Naydenov, J. Beck, F. Rempp, M. Steiner, V. Jacques, G. Balasubramanian, M. L. Markham, D. J. Twitchen, S. Pezzagna, J. Meijer, J. Twamley, F. Jelezko, and J. Wrachtrup, Quantum register based on coupled electron spins in a room-temperature, Nat. Phys. **6**, 249 (2010).

[32] F. Dolde, I. Jakobi, B. Naydenov, N. Zhao, S. Pezzagna, C. Trautmann, J. Meijer, P. Neumann, F. Jelezko, and J. Wrachtrup, Room-temperature entanglement between single defect spins in diamond, Nat. Phys. **9**, 139 (2013).

[33] H. S. Knowles, D. M. Kara, and M. Atatüre, Demonstration of a Coherent Electronic Spin Cluster in Diamond, Phys. Rev. Lett. **117**, 100802 (2016).

[34] G. Calusine, A. Politi, and D. D. Awschalom, Cavity-Enhanced Measurements of Defect Spins in Silicon Carbide, Phys. Rev. Applied **6**, 014019 (2016).

[35] D. O. Bracher, X. Y. Zhang, and E. L. Hu, Selective Purcell enhancement of two closely linked zero-phonon transitions of a silicon carbide color center, Proc. Natl. Acad. Sci. USA **114**, 4060 (2017).

[36] B. S. Song, S. Yamada, T. Asano, and S. Noda, Demonstration of two-dimensional photonic crystals based on silicon carbide, Opt. Express **19**, 11084 (2011).

[37] L. Marseglia, J. P. Hadden, A. C. Stanley-Clarke, J. P. Harrison, B. Patton, Y.-L. D. Ho, B. Naydenov, F. Jelezko, J. Meijer, P. R. Dolan, J. M. Smith, J. G. Rarity, and J. L. O'Brien, Nanofabricated solid immersion lenses registered to single emitters in diamond, Appl. Phys. Lett. **98**, 133107 (2011).

[38] T. M. Babinec, B. J. M. Hausmann, M. Khan, Y. Zhang, J. R. Maze, P. R. Hemmer, and M. Loncar, A diamond nanowire single-photon source, Nat. Nanotechnol. **5**, 195 (2010).

[39] M. Radulaski, M. Widmann, M. Niethammer, J. L. Zhang, S. Y. Lee, T. Rendler, K. G. Lagoudakis, N. T. Son, E. Janzen, T. Ohshima, J. Wrachtrup, and J. Vučković, Scalable quantum photonics with single color centers in silicon carbide, Nano Lett. **17**, 1782 (2017).